Simulations of the Boundary Layer Between a White Dwarf and its Accretion Disk

Dinshaw S. Balsara & Jacob Lund Fisker

Department of Physics, University of Notre Dame, Notre Dame, IN 46556
dbalsara@nd.edu; jfisker@nd.edu

Patrick Godon[1] & Edward M. Sion

Department of Astronomy and Astrophysics, Villanova University, Villanova, PA 19085
patrick.godon@villanova.edu; edward.sion@villanova.edu

ABSTRACT

Using a 2.5D time-dependent numerical code we recently developed, we solve the full compressible Navier-Stokes equations to determine the structure of the boundary layer between the white dwarf and the accretion disk in non-magnetic cataclysmic variable systems. In this preliminary work, our numerical approach does not include radiation. In the energy equation, we either take the dissipation function (Φ) into account or we assume that the energy dissipated by viscous processes is instantly radiated away ($\Phi = 0$). For a slowly rotating non-magnetized accreting white dwarf, the accretion disk extends all the way to the stellar surface. There, the matter impacts and spreads towards the poles as new matter continuously piles up behind it. We carry out numerical simulations for different values of the alpha viscosity parameter (α), corresponding to different mass accretion rates. In the high viscosity cases ($\alpha = 0.1$), the spreading boundary layer sets off a gravity wave in the surface matter. The accretion flow moves supersonically over the cusp making it susceptible to the rapid development of gravity wave and/or Kelvin-Helmholtz shearing instabilities. This BL is optically thick and extends more than 30 degrees to either side of the disk plane after only 3/4 of a Keplerian rotation period (t_K=19s). In the low viscosity cases ($\alpha = 0.001$) , the spreading boundary layer does not set off gravity waves and it is optically thin.

Subject headings: accretion, accretion disks – binaries: close — novae, cataclysmic variables — white dwarfs — methods: numerical

[1]Visiting at the Space Telescope Science Institute, Baltimore, MD 21218, USA, godon@stsci.edu

1. Introduction: Accreting White Dwarfs in Cataclysmic Variables

Cataclysmic variables (CVs) form an interesting class of short-period close binary systems comprising a hot white dwarf (WD) and a relatively lower mass red dwarf star filling its Roche lobe (Crawford & Kraft 1956; Kraft 1962). In such systems hydrogen-rich matter from the red dwarf exits through the inner Lagrange point (L1) and flows towards the white dwarf. In the absence of strong magnetic fields, the matter forms an accretion disk around the white dwarf due to the excess angular momentum originating from the orbital motion of the binary (Prendergast & Burbidge 1968; Flannery 1974; Lubow & Shu 1975). On-going accretion at a low rate (quiescence) is interrupted every few weeks to months by intense accretion (outburst) of days to weeks - a dwarf nova (DN) accretion event (Bath 1972), thereby increasing the luminosity of the systems by several magnitudes. A thermal instability in the accretion disk is believed to trigger the increase in the mass transfer rate ($\dot{m}$) through the disk and thus an increase in the rate of gravitational energy release (Cannizzo et al. 1988).

CV systems are divided in sub-classes according to the duration, occurrence and amplitude of their outburst (Hack & la Dous 1993; Warner 1995; Ritter & Kolb 1998): e.g. dwarf nova systems (DNs) are non-magnetic and accrete through a disk, they spend most of their time in the quiescent state; nova-like systems (NLs) are disk-systems found mostly in the high outburst state; polars are devoid of an accretion disk due to their strong magnetic fields (the matter is funneled through the magnetic field lines onto the poles of the WD); and intermediate polars (IPs) have truncated inner disks due to their moderately strong magnetic fields. Another CV subclass is the classical nova (or just "nova";), characterized by an episode of unstable thermonuclear burning (the thermonuclear runaway - TNR; Rose (1968)). All CV system are believed to undergo a classical nova explosion every few thousand years or more, when enough hydrogen-rich material accumulated in the envelope to reach the ignition point at the electron-degenerate base of the envelope - where it is compressed under the large gravity of the WD (Starrfield 1971a,b; Starrfield et al. 1972). In the present work we concentrate on the study of the non (or weakly) magnetized DN systems, where the accretion disk extends all the way to the surface of the WD.

Since the white dwarf is the most common end-product of stellar evolution ($\approx 90\%$ of all the stars in the Galaxy have evolved or will evolve into white dwarfs) and the accretion disk is the most common universal structure resulting from mass transfer with angular momentum, and both can be directly observed in cataclysmic variable systems (in the ultraviolet), an understanding of the accretion process in cataclysmic variables is the first step in a global understanding of accretion in other systems throughout the universe. These include young stellar objects, accretion onto neutron stars and black holes, and the most difficult to study, active galactic nuclei. Therefore, accreting white dwarfs in cataclysmic variables are the best

astronomical laboratories to study the physics of accretion disks.

1.1. The Accretion Disk & Boundary Layer in One-Dimension

In the disk, magneto-hydrodynamic (MHD) turbulence (Shakura & Sunyaev 1973) due to a magneto-rotational instability (Balbus et al. 1994) dissipates potential energy and transfers angular momentum outward. As a result, the disk matter slowly spirals inwards towards the white dwarf (Pringle 1981). The total potential energy of accretion can be released at the maximum rate

$$L_{acc} = \frac{GM_*\dot{m}}{r_*} = \dot{m}r_*^2\Omega_K^2(r_*), \tag{1}$$

where G is the gravitational constant, M_* is the mass of the WD, r_* its radius, $\dot{m}$ is the mass accretion rate, and $\Omega_K(r_*)$ is the Keplerian angular velocity at one stellar radius r_*. This is the maximum amount of energy that can be extracted from the accretion process per unit of time and the actual luminosity can be smaller than this (see below). In the standard disk theory (Shakura & Sunyaev 1973; Lynden-Bell & Pringle 1974), the accretion disk is axisymmetric, geometrically thin in the vertical dimension (it has a thickness H such that $H/r << 1$), and the energy dissipated by the (turbulent) viscosity is instantly radiated locally in the $\pm z$ directions. Only half of the accretion luminosity is emitted by the disk ($L_{disk} = L_{acc}/2$), since the matter is still moving at a nearly Keplerian velocity, $v_K \approx \sqrt{GM_*/r_*}$, before it is ultimately accreted (Lynden-Bell & Pringle 1974).

The remaining accretion energy must, therefore, be dissipated in order for the matter to be accreted onto the surface of the more slowly rotating WD (Pringle 1981). The disk matter is decelerated in that region where the inner disk reaches the stellar surface: the boundary layer (BL). The height of the BL can be comparable to the scale height H of the accretion disk. The remaining rotational kinetic energy of the accreting matter dissipated in the boundary layer per unit of time (L_{BL}) is nearly equal to half of the total luminosity of the accreting matter (L_{acc}), namely:

$$L_{BL} = \left(1-\beta^2\right) L_{disk} = \frac{\dot{m}r_*^2}{2}(\Omega_K^2(r_*) - \Omega_*^2), \tag{2}$$

where $\beta = \Omega_*/\Omega_K(r_*)$, and Ω_* is the stellar angular velocity. This is so because the material accreted onto the WD surface corotates with it and keeps a fraction of the rotational kinetic energy. Kluźniak (1987), however, pointed out that part of the BL energy goes into spinning up the accreting star through the shear at the stellar equator, and hence, the fraction that

can be radiated away is smaller than the one given in eq.(2). Namely, one has

$$L_{BL} = (1-\beta)^2 L_{disk} = \frac{\dot{m} r_*^2}{2}(\Omega_K(r_*) - \Omega_*)^2. \quad (3)$$

Therefore, for a non-rotating WD: $L_{BL} = L_{disk} = L_{acc}/2$. However, for a rotating WD $L_{BL} < L_{disk}$, and the total energy radiated from the accretion process ($L_{BL} + L_{disk}$) is actually smaller than L_{acc} as defined by eq.(1). The energy "kept" by the corotating accreted material per unit of time is :

$$\beta^2 L_{disk} = \frac{\dot{m} r_*^2}{2}\Omega_*^2, \quad (4)$$

and the power invested to spin up the star through the shear at the equator (eq.2-eq.3) is:

$$[(1-\beta^2) - (1-\beta)^2] L_{disk} = 2\beta(1-\beta) L_{disk} = \beta(1-\beta) L_{acc}. \quad (5)$$

The above relations are correct to order of $\eta = 1 - r_m/r_*$, where r_m is the radius at which the gradient of the angular velocity changes sign $\partial\Omega/\partial r = 0$ (for further details of the one-dimensional analysis see also Regev (1983); Kley (1991); Popham & Narayan (1995)). Usually η is of the order of H/r or smaller. For a WD star rotating at 10% of the Keplerian velocity (i.e. several 100km/s) the BL is expected to radiate $L_{BL} = 0.81 L_{disk}$, while a fraction of $0.18 L_{disk}$ is invested in spinning up the star. For a WD star rotating at 30% of the Keplerian velocity (i.e. $\sim$ 1000km/s) the BL is expected to radiate $L_{BL} = 0.49 L_{disk}$. For a star rotating near break-up the angular velocity in the disk does not have an extremum and decreases steadily outward, therefore the disk is expected to spin-down the fast rotating WD (Popham & Narayan 1991). In this case there is no boundary layer.

Since the BL is much smaller than the disk itself and each radiate almost equal amounts of energy, the disk emits mainly in the optical and near UV, whereas the much hotter BL emits in the far UV and in X-rays. During outburst, when $\dot{m} \approx 10^{-9} - 10^{-8} M_\odot$/yr (Warner 1987; Cannizzo et al. 1988), observations (e.g. Córdova et al. (1980); Mauch et al. (1995); Mauche (2004)) reveal that the BL is optically thick and emits mainly in the FUV and soft X-ray bands with an effective temperature T_{eff} of a few 10^5K as expected by the theory (Pringle & Savonije (1979); Regev (1983); Godon et al. (1995); Popham & Narayan (1995); Collins et al. (1998); Obach & Glatzel (1999)). During quiescence, when $\dot{m} \approx 10^{-12} - 10^{-10} M_\odot$/yr (Warner 1987), observations (e.g. Mukai & Patterson (2004); Pandel et al. (2003, 2005)) reveal that the boundary layer is optically thin and emits in the hard X-ray band with a temperature of the order of 10^8K, as expected by the theory (e.g. Pringle & Savonije (1979); Tylenda (1981); King & Shaviv (1984); Shaviv (1987); Narayan & Popham (1993); Popham (1999)). However, in addition, in the outer region of the BL, where the BL meets the disk, the optical thickness becomes larger again (~ 1) and that region emits in the FUV with a temperature T_{eff} reaching $\sim 10^5$K (Popham 1999).

1.2. Observational Background

Observationally, it was shown almost three decades ago that non-magnetic CVs do emit some fraction of their luminosity in the X-ray bands (e.g. Córdova et al. (1980, 1981); Becker & Marshall (1981); Córdova & Mason (1983); Patterson & Raymond (1985); the ROSAT All-Sky Survey (Beuermann & Thomas 1993)). As expected from the one-dimensional standard disk and boundary layer theories, during quiescence hard X-rays (10keV and higher) were observed from a small region close to the WD (e.g. van Teeseling et al. (1996); Mukai et al. (1997)), while during outburst this emission is replaced by soft X-ray and EUV (see e.g. the review of Mauche (1996) and the references therein). The EUV region of the spectrum is very difficult to observe because the absorption cross section of (ISM) neutral hydrogen is very high. Because of this, only a few systems have been successfully observed in the EUV, such as e.g. VW Hyi (Mauche et al. (1991); for which $N(H) \sim 6 \times 10^{17}\mathrm{cm}^{-2}$, Polidan et al. (1990)). Assuming that the X-ray and EUV emissions are from the BL, and the optical and UV emissions are from the disk, many previous studies found a very low ratio L_{BL}/L_{disk} ($\approx 0.001 - 0.04$, Mauche et al. (1991); Hoare & Drew (1991)) during outburst, and a ratio of $L_{BL}/L_{disk} \approx 0.25$ in quiescence (e.g. for VW Hyi, Belloni et al. (1991) assuming that the WD contributes 50 percent of the UV flux). The X-ray observations of *underluminous* boundary layers culminated with the *ROSAT* observations of ten cataclysmic variables (BA Cam, YZ Cnc, GP Com, VW Hyi, WX Hyi, TY PsA, V3885 Sgr, CY UMa, CY Vel, IX Vel) by van Teeseling & Verbunt (1994), in which 8 systems were caught in quiescence and 2 systems were caught in outburst. van Teeseling & Verbunt (1994) derived X-ray fluxes from their observations and UV fluxes from existing *IUE* observations and found that ratio of the X-ray Luminosity to the UV+Optical Luminosity is much smaller than one.

Many processes were discussed to explain the "missing boundary layer" (e.g. Ferland et al. (1982); Shaviv (1987); King (1997); Meyer & Meyer-Hofmeister (1994); Ponman et al. (1995)). The main idea was that the kinetic energy of the BL could also be converted into winds (e.g. King & Shaviv (1984)), WD or belt rotation (e.g. Kippenhahn & Thomas (1978)), heating (e.g. Shaviv & Starrfield (1987); Regev & Shara (1989); or maybe advected into the outer stellar envelop (e.g.. Godon (1996a, 1997b); Popham (1997)). Some systems have been observed to have a WD rotating at a rather large rotational velocity, of the order of $\sim 1,000$km/sec (e.g. Cheng et al. (1997); Pandel et al. (2005)), which implies (from eq.3) $L_{BL}/L_{disk} = 1/2$. However, the observed X-ray luminosities have been much smaller than this and would imply a near-Keplerian rotation rate for many systems, which is not the case.

Recent XMM-Newton observations (Pandel et al. 2005), taking into account the contribution of the disk, WD and BL in the optical, UV and X-ray bands, found no evidence of

an underluminous BL in 8 quiescent dwarf novae (OY Car, WW Cet, AB Dra, U Gem, VW Hyi, T Leo, TY PsA, SU UMa) and the data are consistent with $L_{BL} \approx L_{disk}$. The main difference with previous studies was that the WD contribution was taken into account with realistic temperatures taken from the literature and could dominate over the disk in the UV. Pandel et al. (2005) basically assumed $L_{disk} = L_{UV} + L_{opt} - L_{WD}$ and $L_{BL} = L_X$, and found $L_{BL}/L_{disk} \sim 1$ for 6 objects among 8. For VW Hyi and U Gem (with $L_{BL}/L_{disk} \sim 1/3, 1/2$ respectively) they suggest that the inner disk is truncated at $r \sim 3R_{WD}$ to explain the discrepancy.

Godon & Sion (2005) further computed the contribution of all the emitting components (WD, disk, BL) in the optical, UV and X-ray based on the existing multiwavelength observations of VW Hyi, the standard disk model (Pringle 1981) and Popham (1999)'s model of the boundary layer. Popham (1999) has shown that (in quiescence) the BL emits part of it energy in the UV band from that region where the outer edge of the BL meets (and radiates energy into) the optically thick inner edge of the disk. Godon & Sion (2005) suggested that the second component often observed in the quiescent UV spectra of DNe (the so-called accretion belt also detected in the *FUSE* spectra of VW Hyi — (Godon et al. 2004b)) is the UV emission from the outer BL. Taking the UV contribution of this second component (L_{2nd}) into account Godon & Sion (2005) showed that the luminosity of the BL of VW Hyi in quiescence ($L_{BL} = L_X + L_{2nd}$) is as expected from the theory (namely $L_{BL} = L_{disk} = L_{opt} + L_{UV} - L_{WD}$), therefore agreeing with Pandel et al. (2005) that *there is no missing boundary layer* even for VW Hyi and without disk truncation.

On the other hand, spectroscopic UV observations of accreting WDs have also reached a rather advanced stage. Observations have been carried out for a range of CVs, (Long et al. 1993; Froning et al. 2001; Szkody et al. 2002; Welsh et al. 2003; Sion et al. 2005; Godon et al. 2004a, to cite just a few) in quiescence and outburst. The observations suggest that the spectrum is made up of several parts, specifically, the underlying WD, the accretion disk, the accretion belt that might form on the surface of the star, the hot spot (where the matter inflowing from the L1 point hits the outer rim of the accretion disk). The temperature of each of these components proves to be a most important diagnostic, though as better data come in, we can hope that other hydrodynamical variables also become important diagnostics. The case of VW Hydri is especially important because STIS measurements (Sion et al. 2005) have captured that object during its transition to outburst. The VW Hyi transition to outburst caught by *STIS* was apparently an outside-in outburst. The UV lagged the optical. The *STIS* showed that longer FUV wavelengths changed much faster and manifested the flux sooner than shorter wavelengths. It has been found that the temperature of the accreting star can be raised by as much as 50% during outburst. The elevated WD temperature returns to its quiescence value soon after the outburst. The elevated surface temperature

of the star may, therefore, be a good diagnostic of the energy dissipated as the accretion stream impacts, spreads out and slows down and reaches co-rotation with the star. The rate at which the WD cools following the heating during the outburst is not only diagnostic of the mass/depth of the heated surface layers but also potentially a good diagnostic of the optical depth of the accreted material. A detailed understanding of BL physics may also help one understand the so-called UV delay where the rise in the UV emission lags the rise in the optical by several hours, indicating that the UV emission might be more symptomatic of the physics of the BL (Livio & Pringle 1992). It is important to note here that our present numerical simulations are relevant to the changes in the WD temperature observed on a time scale of the order of outburst/quiescence cycle (e.g. VW Hyi), and do not apply to compressional heating taking place on a much longer evolutionary time scale (Sion 1995; Godon & Sion 2002, 2003; Piro et al. 2005).

1.3. The Two-Dimensional Boundary Layer

The BL has typically been solved in a model where the averaging of the vertical structure which is employed in accretion disk studies (Shakura & Sunyaev 1973) has been extrapolated to the surface. One also makes the additional simplifying assumption that the vertical velocity in the boundary layer is zero, just as it is in the outer parts of a thin disk model. This reduces the description of the BL to a one dimensional problem in the radial direction (Pringle 1981; Meyer & Meyer-Hofmeister 1982; Popham & Narayan 1995; Collins et al. 1998), where one actually solves the "slim disk" equations for the BL region (namely, the one-dimensional disk equations + radiation in the radial direction; as first proposed in the pioneering work of Regev (1983)). However, this assumption is not necessarily correct since the BL may spread out (Ferland et al. 1982). The best one-dimensional models of the BL (Popham & Narayan 1995) predict a rise in the BL temperature during outburst that is much larger than the observed one.

Recognizing the multi-dimensionality of the problem several authors attacked the problem directly using numerical methods (e.g. Robertson & Frank (1986)) culminating in simulations which included flux-limited radiative transport as well as different viscosities (Kley & Hensler 1987; Kley 1989, 1991). However, while the efforts of Kley & Hensler (1987); Kley (1989, 1991) were very bold and impressive, the high numerical resolution needed to solve the problem has until now precluded following the problem numerically on a long evolution time scale and or resolving the fine structure of the flow. The importance of the meridional flow was demonstrated in protostars and FU Ori stars already by Kley & Lin

(1996, 1999), who show how matter spread to the poles to completely engulf the accreting star. However, in accretion onto a compact star the problem has not been solved because of the much smaller scales.

As the numerical two-dimensional simulations failed to follow the evolution of the accretion onto the surface of the compact star, an analytical approach was developed by Inogamov & Sunyeav (1999), who implemented the one-dimensional BL equations with an analytic treatment of the meridional direction (assuming a shallow-water equation), where the vertical velocity in the boundary layer is permitted to be non-zero. This analytical treatment was carried out for an accreting neutron-star (NS), and it was shown that the BL could "spread" and cover a significant part of the NS. Later on, (Piro & Bildsten 2004a) applied Inogamov & Sunyaev's treatment of the "spread layer" to accreting white dwarf in outburst (the optically thick case). The analytical work of Piro & Bildsten (2004a) indicates that the numerical setup must include sufficient resolution in the radial and meridional planes to capture the dynamics and fine structure of the BL. It is the purpose of the present simulations to actually provide such a numerical study, by following the evolution of the accretion onto (and into!) the surface of the WD in the inner region of the disk and close to the equatorial plane ($i < 30$deg).

In the one dimensional picture the energy kept by the corotating accreted material per unit time is given by eq.4. In two dimension, however, as the matter possibly spreads evenly onto the WD surface, its moment of inertia is rather similar to that of a spherical shell and the energy kept by the accreted material per unit of time becomes

$$\frac{1}{2}\Omega_*^2\frac{2}{3}\dot{m}r_*^2 = \frac{2}{3}\beta^2 L_{disk}, \tag{6}$$

and the remaining energy (eq.4)-(eq.6)

$$\frac{1}{3}\beta^2 L_{disk} \tag{7}$$

is available to further spin up the WD. As the matter moves toward the poles, to spread evenly on the WD surface, it has excess of angular velocity/momentum (due to the differential velocity) which is added to the accreting WD. We therefore see that even for the most simplistic two-dimensional model of the boundary layer, the spreading of matter on the WD surface involves a significant fraction of the accretion energy (e.g. up to 10% of the disk luminosity for a star rotating at 1,000km/sec — eq.7). In the case of a star rotating near break-up velocity, accretion at the equator *adds angular momentum to the star as the matter spreads toward higher latitudes*. This contributes to a balancing effect to the spin-down of the an accreting star rotating near break-up as described by Popham & Narayan (1991).

1.4. The Importance of the Boundary Layer

The structure of the BL is important to help disentangle and physically characterize the different emitting components in an accreting WD system. The details of the emitted spectrum depends sensitively on the detailed structure of the boundary layer and how it changes in response to enhanced rates of accretion (Fisker & Balsara 2005). The boundary layer is also important because it may play a role in the still uncertain mechanism which drives the outflowing bi-polar winds seen in dwarf novae during outburst and in nova-like variables during their high optical brightness states. Our boundary layer simulations will eventually provide the theoretical framework required to physically interpet the X-ray, EUV and FUV emission observed in compact binaries containing accreting degenerate stars.

However, the structure of the BL is also important because it determines how the accreted matter ultimately distributes itself in the envelope of the WD, which is important for classical novae. In classical novae, the thermonuclear runaway (TNR) ejects part or all of the envelope. The initial CNO composition of the burning material should be strongly enhanced compared to the accreted material to account for composition of the observed ejecta (Starrfield et al. 1972). Several mechanisms have been suggested for this CNO enhancement (see José (2005) and references therein). They can be roughly divided into pre-burst mixing between accreted material and the underlying CO rich WD (Kippenhahn & Thomas 1978; MacDonald 1983; Rosner et al. 2001; Alexakis et al. 2004) by accretion driving instabilities or mixing with the underlying material when the convective zone of the thermonuclear runaway extends deep enough to dredge up CO material (Starrfield et al. 1972; Glasner et al. 1997).

However, before an exploration of the radiation emission characteristics of the boundary layer can be carried out with full radiation hydrodynamics, we must understand the dynamical processes that lead to the formation of the boundary layer. In this first stage our goal is to calculate the dynamical structure of the boundary layer with sufficient numerical resolution to capture the dynamical evolution of the accretion flow and its interaction with the stellar surface (see Fisker & Balsara (2005)), and we leave the radiation-hydrodynamical study for later.

Our model is presented in section 2, the results are given and discussed in section 3. Section 4 presents the conclusions. The equations we are solving are written down explicitly in Appendix A while the initial and boundary conditions are described in Appendix B.

2. Computational model

The source of the angular momentum transport in the BL probably involves a combination of magnetic fields and turbulence. Since the angular velocity in the BL is not a decreasing function of radial distance from the star, it is not clear that the magnetorotational instability (MRI) (Balbus et al. 1994) provides angular momentum transport in the BL. Actually, Brandenburg et al. (1996) found that the effective alpha viscosity parameter α would go to zero for a rotation law $\Omega \sim r^{-q}$ when $q < 0$. Nor is the MRI essential at the BL because the accretion disk can directly exchange angular momentum and mass with the outer layers of the star if an efficient coupling mechanism is found between the disk and the star. The source of viscosity at the BL is still debated in the literature (see Popham & Narayan (1995); Piro & Bildsten (2004a); Godon & Sion (2005)). Inogamov & Sunyeav (1999) assumed that the viscosity is due to purely hydrodynamical turbulence as in the deceleration of subsonic or supersonic flow above a solid surface. The case for a purely hydrodynamical turbulence in the boundary layer was already debated earlier (Zahn 1990; Dubrulle 1993), however the physical process is likely to take place in three dimensions (Orszag & Kell 1980), e.g. by means of streamwise vortices (e.g. Hamilton & Habernathy (1994)). The most common instability in a flow over a *curved surface*, is that of the boundary layer flow over a concave surface unstable to the centrifugal instability (as it violates Rayleigh's criterion for stability — (Rayleigh 1916)). This instability leads to turbulence through the formation of the Görtler vortices (Saric 1994), which tap energy from the laminar flow and poor it into the turbulence (this is a non-linear instability leading to a subcritical transition to turbulence). However, the boundary layer flow on a convex surface is not subject to this instability, rather the opposite, the centrifugal force in such a flow is "restoring". Therefore, the instability that is the most likely to take place in the star-disk boundary layer is the Kelvin-Helmhotz shearing instability which will occur for a sufficiently large shear (Richardson criteria, e.g. Drazin & Reid (1981)).

Following (Shakura & Sunyaev 1973) , we parametrize the efficiency of the angular momentum transport with an α viscosity prescription. In a multidimensional calculation α has to be spatially concentrated at the accretion disk and the stellar surface and the formulations developed in (Papaloizou & Stanley 1986) and (Kley 1991) are used here. Specifically, we used $\nu = \alpha c_s min(H, h_p)$ where H is the scale height of the disk and h_p is the local pressure scale height in the boundary layer. For these calculations, the pressure scale height in the boundary layer that develops on the surface of the star is always smaller than the scale height of the disk. The compressible Navier-Stokes equations themselves are written explicitly in the Appendix A. Describing the angular momentum transport with a simple shear coefficient means that the dynamics follows the Navier-Stokes equations. Here the Navier-Stokes equations as given by Mihalas & Mihalas (1984) are solved in spherical co-

ordinates (r,θ,ϕ) on an axisymmetric mesh with 384 ratioed zones in the radial direction and 128 ratioed zones in the meridional range spanning 0 to 30 degrees from the disk plane – same as Fisker & Balsara (2005). The star was taken to be a non-rotating $0.6M_{\odot}$ WD with a radius of $9 \times 10^8 cm$. The radial extent of our computational domain extended from $8.9 \times 10^8 cm$ to $1.1 \times 10^9 cm$. The r-directional zones were concentrated towards the inner radial boundary with each zone being 1% larger than the previous one. The θ-directional zones were also ratioed with the smallest zones being closest to the equator and each zone being 1.9% larger than the previous one. Such a ratioed zoning makes it possible for us to capture five scale heights of the star's atmosphere as well as the vertical structure of the disk. The zone ratioing also concentrates zones around the disk-star interface. Unlike (Kley 1991) , who used a mesh with 85 zones in each of the radial and meridional directions, our mesh has substantially better resolution. The scale heights of WD atmospheres are now known to be substantially smaller than estimated in (Kley 1991; Kley & Hensler 1987), making the larger meshes used in this work more essential. The higher resolutions, as well as the use of higher order Godunov methods, enable us to substantially reduce the role of numerical diffusion.

In this paper, we wish to study not just the spin-down of the accretion disk but also the spin-up of the star. For that reason, we retained five scale heights of the WD's outer atmosphere. Care was taken to resolve each stellar scale height in the radial direction with at least twenty zones, which ensures a numerically accurate, well-resolved and stable stellar atmosphere. To ensure good resolution of the disk's structure, we retained at least fifty zones across a disk scale height in the meridional direction. The physical conditions describing the structure of the disk are given in Appendix B. Typical surface temperatures for hydrodynamically accreting WDs are $\sim$ 30,000K and typical disk temperatures are usually taken to be $\sim$ 100,000K. This choice of temperatures would make the scale heights of the disk and WD atmosphere too small to be resolved with the above-mentioned resolutions. For this reason, we systematically allow the temperatures of both the disk and WD atmosphere to be one order of magnitude larger than the physical values. As a result, the simulations were carried out with a stellar temperature of T=300,000K and a disk temperature of T=1,000,000K. While this might seem be a hot temperature for a disk in a CV, it is still much less than the virial temperature and the corresponding disk thickness is $H/r = 0.03$ instead of $H/r = 0.01$ for a 10^5K disk. The sound speed used in the formulae for the viscosity ν was derived for the temperatures used in the simulations. We assume a very tenuous and very hot halo which consists of the same material as the disk (and the star). The mass in this halo is extremely small, making the halo dynamically unimportant and its sole use is to provide pressure balance at the upper boundaries of the accretion disk and the star. The fluids that make up the disk, halo and stellar atmosphere were tagged with passive scalars and we are,

therefore, in a position to assert that the halo gas simply provides pressure support with minimal mixing into the gas that makes up the disk or the stellar atmosphere. Such a model with a disk and halo that are in dynamical equilibrium with each other was briefly described in Balsara (2004). Since that previous work did not include the stellar atmosphere, appendix B describes the physical conditions that were assumed to set up the WD atmosphere, the accretion disk and the halo. Symmetry across the disk plane is assumed.

Observations, and their interpretation in the context of the Popham & Narayan (1995) model have suggested that the interesting values of α range from 0.1 during outburst to 0.001 during quiescence. Godon & Sion (2005) derived $\alpha = 0.004$ in the boundary layer from the XMM-Newton observations of VW Hyi in quiescence (Pandel et al. 2003). For that reason, we performed a parameter study with $\alpha = 0.1$, $\alpha = 0.03$, $\alpha = 0.01$, $\alpha = 0.005$, and $\alpha = 0.001$. The same value of α was used in the boundary layer and in the disk. This would seem to be a very reasonable assumption if the same physical mechanism (such as a thermal instability, Cannizzo (1998) or magnetic instability Livio & Pringle (1998)) were to make the disk fluid and the boundary layer fluid turbulent. Our simulations do not include the effect of radiative transfer in the boundary layer. It is worth noting that in the optically thick limit, the BL retains most of the energy that is generated by the viscous stresses. As a result, by retaining the viscous energy generation terms in eq. [A5] and assuming that the alpha viscosity parameter is large ($\alpha \sim 0.1$) we mimic the situation where the boundary layer is optically thick during outburst. Simulations were also carried out by excluding the viscous energy generation terms in eq. [A5] and assuming $\alpha \sim 0.001$; in that situation we mimic the limit where the boundary layer is optically thin during quiescence, i.e. the BL radiates away all the heat that is generated by the viscous stresses. Our results, therefore, bracket the two extreme cases. Should the high α simulations produce BLs with optical depths in excess of 50 or 100 , the optically thick runs would find direct applicability to the astrophysical problem. Likewise, should the low α simulations produce optically thin boundary layers, the optically thin runs would find direct applicability to the astrophysical problem. We show in the course of this work that such trends are indeed observed in the simulations. In future work, we will include a treatment of the radiative transfer terms in the BL thus obtaining results that are free of current limitations. The full range of simulations that we report on here with the various values of α and the inclusion or exclusion of viscous energy generation terms are listed in Table 1.

Since the inner radial boundary extends into the star, we enforced reflective boundary conditions at that boundary. While such a boundary condition would reflect any waves that reached the star's surface, we find that in practice the waves do not propagate to this depth in the present simulations. The use of such a reflective boundary condition represents a compromise. While it might reflect back waves that propagate more than five scale heights

into the star, our experience has shown that surface waves almost never propagate to that depth. The present boundary conditions do have the positive consequence that they prevent any unexpected mass or momentum inflow into the computational domain from the rest of the star. The outer radial (computational) boundary was designed to respond to inflow or outflow of fluid at the outer open boundary, and it was therefore treated by imposing the boundary conditions on the characteristics of the flow as described in (Godon 1996b). Thus outer boundary conditions were imposed directly on the incoming characteristics, and computed values from the variables inside the domain were imposed (propagated) on the outgoing characteristics. The strategy works well, especially when combined with Riemann solvers which also work on the same principle of resolving the inflowing and outflowing waves. The equatorial boundary condition in the θ-direction was reflective (symmetric) and the boundary condition at the other θ-directional boundary was specified as continue.

model	α	Φ
v1	0.1	yes
v2	0.03	yes
v3	0.01	yes
v4	0.005	yes
v5	0.001	yes
nv1	0.1	no
nv2	0.03	no
nv3	0.01	no
nv4	0.005	no
nv5	0.001	no

Table 1: This table shows our ten models. The first column indicates the model name. The second column indicates the α-viscosity employed in the model and the last column shows whether dissipative heating was included in the model.

The spatially and temporally second order algorithms in `RIEMANN` have been described in Roe & Balsara (1996); Balsara (1998a,b); Balsara & Spicer (1999a,b); Balsara (2004) and use many ideas from higher order WENO schemes (see Jiang & Shu (1996); Balsara & Shu (2000)) to reduce dissipation. The matter in the model is subject to the central gravitational field of the underlying WD. The model uses an ideal gas ($\gamma = 5/3$) of a fully ionized solar composition ($\mu = 0.62\,\mathrm{g/mole}$) and assumes no radiative transport.

3. Results and Discussions

In the next subsections, we focus on several important aspects of the boundary layer dynamics as follows. In section 3.1 we focus on the density profile of the boundary layer. In section 3.2 we consider the pressure profiles in the boundary layer. In section 3.3, we focus mainly on the the evolution of angular momentum in the boundary layer . In section 3.4 we check the stability of the flow in the boundary layer. In section 3.5, we discuss accretion based instabilities and in section 3.6 we relate the computations to observations.

3.1. Density Structure of the Boundary Layer

Figs 1a and 1b show the logarithm of the density in the boundary layer with $\alpha = 0.1$ and $\alpha = 0.001$ respectively. Figs 1c and 1d and do the same for the runs with the same values of α but with the viscous heating switched off in eq. [A5]. The full extent of the computational domain is shown in the θ-direction. Only a small portion of the inner radial direction is shown and the values on the x-axis of the plot are in units of $10^9 cm$, making it possible to measure the radial coordinate . The same convention for labeling figures applies to all other figures in this paper where flow variables are imaged.

In all cases, the poloidal velocity is overlaid as vectors, enabling us to trace the flow of matter on the surface of the star. Thus Fig. 1a pertains to the optically thick limit

Fig. 1.— (a) left panel. The logarithmic density for model v1 is shown after one Keplerian rotation. (b) right panel. The logarithmic density for model v5 is shown after one Keplerian rotation. (c) next page - left panel. The logarithmic density for model nv1 is shown after one Keplerian rotation. (d) next page - right panel. The logarithmic density for model nv5 is shown after one Keplerian rotation. The full extent of the computational domain is shown in the θ-direction. Only a portion of the radial direction is shown and the values on the x-axis of the plot are in units of $10^9 cm$, making it possible to measure the radial coordinate.

(outburst state) while Fig. 1d corresponds to the optically thin limit (quiescent state). We see that a thick, dense boundary layer forms in both Figs. 1a and 1c while that is not the case in Figs. 1b and 1d. Thus, physically thick boundary layers form in outburst and the result is independent of whether the viscous energy generation is included in the energy equation. The boundary layers that form in quiescence tend to be physically thin. This shows that the viscosity is the primary discriminant in determining the structure of the BL. The poloidal velocity vectors in Figs 1a and 1c also show us that the velocity increases with increasing distance from the star's surface. The velocity vectors in Figs. 1b and 1d show a similar trend though it is harder to see because of the smaller physical extent of the BL. Such a velocity structure is also known to occur in terrestrial fluid dynamics when a viscous fluid flows over a stationary solid surface, forming a boundary layer at the solid's surface. This shows us that our simulations are producing a valid result which is consistent with our intuition. It also shows us that our decision to refer to these star-disk layers as boundary layers is well-motivated.

The accretion rate is high enough in the $\alpha = 0.1$ cases that the infalling matter depresses the stellar atmosphere close to the equator. While this is not so evident in Fig. 1a–1d, we will show in section 3.5 that the infalling matter can excite gravity waves on the surface of the star. Likewise, in section 3.3 we will show that the high α case spins up a significant portion of the star's atmosphere while itself being spun down. The net result of this process is that the toroidal velocity of the disk becomes sub-Keplerian at larger radii from the star as α increases, resulting in broader boundary layers. Fig. 2 shows the mass accreted as a function of time. This figure was generated by integrating the mass from the disk-star interface to the top of the BL where $dv_\phi/dr \equiv 0$. Fig. 2 shows us that the accretion rate is higher in the high-α cases, as expected. Fig. 2 also shows us that for the high α cases the accretion rate seems to drop off with time. This is entirely a result of the fact that this round of simulations does not include radiative transfer. As a result, the base of the boundary layer heats up, with a corresponding increase in pressure. The radiative cooling times in a real accretion disk are short enough (i.e. even smaller than an orbital time) that the boundary layer would cool down quite rapidly. The consequent pressure reduction would then permit accretion to proceed unimpeded.

Because of resolution constraints, we had to use temperatures that are somewhat larger than those that prevail on accreting white dwarfs. In subsequent work, we intend to overcome this constraint. It is, nevertheless, interesting to relate physical depth to optical depth of the boundary layer. In doing that, it is important to exclude the disk fluid that is spinning

Fig. 2.— The mass accretion is shown as a function of time for models v1–v5.

close to the Keplerian velocity. We, therefore, define the disk-boundary layer interface as the region where the gradient of the angular velocity vanishes: $\partial\Omega/\partial r = 0$ at $r = r_m$. In the boundary layer ($r < r_m$) the matter is spinning with a toroidal velocity that is smaller than the Keplerian velocity. For that sub-Keplerian accreted material, we plot the optical depth due to Thompson scattering as a function of meridional angle in Fig. 3. Here we define the optical depth as $-\int_{\infty}^{0} \kappa\rho_{disk} dr$, where $\kappa = 0.34\,\mathrm{g\,cm^{-3}}$ is the Thomson scattering opacity of a fully ionized solar composition. This constitutes the minimum amount of scattering and thus provides a lower bound of the opaqueness of the matter.

The boundary layer is technically defined by the radius where the radial gradient of the accretion flow's angular velocity disappears. We use that definition for the rest of this paper. Because we track the fluids that make the disk, halo and star, we are in a position to isolate just the disk material that is within the boundary layer. The optical depth of this material (in the radial direction) is very important because it sets the emission characteristics of the accretion belts that have been identified in the observational literature. Fig. 3 shows us that physically thick boundary layers in the high-α limit also tend to be optically thick while physically thin boundary layers in the low-α limit tend to be optically thin. The physical implication of that is that during outburst the BL could suppress the emission from a fraction of the star's surface. If the BL is optically thick with an optical depth $\gg 1$ then the hottest part of the boundary layer, which prevails at the disk-star interface would not be visible. However, during both the transitions, from outburst to quiescence and vice-versa, it is possible that this hot layer might become visible, giving one a direct view of boundary layer heating. This might show up as an additional UV component such as the one seen by Sion et al. (2005) in VW Hydri during its transition from quiescence to outburst. A similar UV component has been detected in U Gem by Long et al. (1993); Froning et al. (2001); Szkody et al. (2002) during its transition from outburst to quiescence. Obtaining matched measurements of the velocity and UV excesses would allow one to further corroborate the scenario presented here. We see that the model in Fig. 1a produces an optically thick boundary layer during outburst. It is, therefore, consistent with our claim in Section 2 that inclusion of the viscous dissipation term in eq. [A5] provides a rather realistic representation of the structure of the boundary layer in outburst. Likewise, the model in Fig. 1d, results in an optically thin boundary layer during quiescence. It is thus consistent with our claim that excluding the viscous dissipation term in eq. [A5] is similarly more representative of the structure of the boundary layer in quiescence.

Fig. 3.— The optical depth along the radial direction is shown for models v1–v5 as a function of the angle from the equatorial plane.

3.2. Pressure in the Boundary Layer

Figs 4a and 4b show the logarithm of the pressure in the boundary layer with $\alpha = 0.1$ and $\alpha = 0.001$ respectively. Figs 4c and 4d do the same for the runs with the same values of α but with the viscous heating switched off in eq. [A5].

From Figs. 4a and 4b we see that the pressure of the accreted fluid is highest in the equatorial plane. This high pressure can be attributed to a combination of viscous dissipation as well as the ram pressure due to infall of accreting material. The pressure gradient in the meridional direction on the surface of the star, therefore, drives the meridional flow that develops on the WD's surface. The models that were used in Figs. 4c and 4d did not include viscous heating in eq. [A5]. They, nevertheless, show that the pressure of the accreted fluid is highest in the equatorial plane and in this instance, the increased pressure is entirely attributable to the ram pressure due to infall of accreting material. We also see that the equatorial pressure increase in Fig. 4b is less than that in Fig. 4a and, similarly, for Figs. 4b and 4d. The smaller pressures in Figs. 4c and 4d relative to Figs. 4a and 4b can be attributed to the additional contribution from viscous heating. Fig. 4a–4d, therefore, serves to show us that the formation of the pressure gradient in the meridional direction, which then drives the meridional flow in the boundary layer, is a very commonplace phenomenon. In other words, any flow that is put in a similar geometry and is made to experience similar viscous stresses would naturally form a similar boundary layer, showing the ubiquity of boundary layer formation. (The only other requirement that such a BL flow has to satisfy as the disk material migrates polewards on the star's surface is the ability to lose angular momentum. The next sub-section will show that it can accomplish this very efficiently by spinning up the underlying layers of the stellar atmosphere.) Thus the decision by Inogamov & Sunyeav (1999); Piro & Bildsten (2004a) to include a non-zero meridional velocity in their models was of central importance in forming the inherently multi-dimensional boundary layers that we see in our simulations. Such boundary layers also form in accreting neutron stars, and TTauri stars that are going through the FU Orionis phenomenon Kley & Lin (1996, 1999); Balsara & Fisker (2005).

Fig. 4.— (a) left panel. This figure shows the logarithmic pressure for model v1 after one Keplerian rotation. (b) right panel. This figure shows the logarithmic pressure for model v5 after one Keplerian rotation. (c) next page - left panel. This figure shows the logarithmic pressure for model nv1 after one Keplerian rotation. (d) next page - right panel. This figure shows the logarithmic pressure for model nv5 after one Keplerian rotation.

3.3. Toroidal and Poloidal Velocities

As the simulations start, the shear force transfers angular momentum between differentially rotating disk annuli so that matter can move inwards and accrete on the star at the footpoint of the disk. Angular momentum transfer between the disk material and the stellar surface is also necessary so matter can move to higher latitudes. Otherwise, the centrifugal barrier prevents matter from leaving the footpoint of the disk. It is this transfer of angular momentum which spins up the existing surface layers of the star. Angular momentum is also directly advected onto the star, because the orbiting disk material eventually accretes and forms the new surface.

Fig.5a shows the resulting specific angular momentum after 3/4 of a Keplerian evolution for the $\alpha = 0.1$ case, whereas fig.5b shows it for the $\alpha = 0.001$ case. Fig.5a shows that the halo is spun up as is the underlying star at the footpoint, where the disk connects with the star. Moreover, we observe that by this time in the simulation the disk material has spun up all five atmospheric scale heights of the star at equatorial latitudes. At higher latitudes the spreading disk material is less dense and thus takes longer amounts of time to drag the star's surface around with it. In fig.5b, which is at the same time as fig.5a and uses the same color scale, we see that the disk has not spun up the star's atmosphere even at the stellar equator.

Fig.6 shows the toroidal velocity and sound speed in the disk's midplane as a function of radius for the simulated alpha-viscosities. The cases of $\alpha = 0.01$, $\alpha = 0.005$, and $\alpha = 0.001$ do not show any significant spin-up of the star after 3/4 of a Keplerian rotation, whence there is not significant shear connection between the disk and the stellar surface. Therefore disk matter retains its Keplerian motion much closer to the star which means that even though the accretion rates are smaller, significant amounts of the dissipation can still be generated in the BL close to the star.

The matter in the layers of the star that we simulate is indeed non-degenerate. Even so, the high temperatures cause it to have a rather low specific molecular viscosity. As a result, turbulence and/or threaded magnetic fields might nevertheless be the two most prominent ways to transfer a significant amount of angular momentum to the deeper layers of the WD (Durisen 1973), where the relative motion drives the mixing between the accreted surface material and the deeper layers. A supersonic component in the toroidal direction over most of

Fig. 5.— (a) left panel. A color plot of the specific angular momentum, $\Omega = v_\phi/r$, for the $\alpha = 0.1$ case after 3/4 of a Keplerian rotation period. (b) right panel. A color plot of the specific angular momentum for the $\alpha = 0.001$ case after 3/4 of a Keplerian rotation period.

the BL is obtained for all values of α (see fig.6). The supersonic toroidal velocities mean that the flows are susceptible to the rapid development of gravity wave and/or Kelvin-Helmholtz instabilities in three dimensions. Such instabilities can be studied by taking a small slice of the interface from our simulations and extending it in the toroidal direction in a three dimensional simulation. Our present simulations could then provide the velocities which drive such instabilities. The calculation of the turbulent mixing which obtains from these instabilities must therefore be calculated using other models (Kippenhahn & Thomas 1978; MacDonald 1983; Rosner et al. 2001; Alexakis et al. 2004).

Fig. 7a shows the poloidal Mach number of the accreted material on the surface of the star for $\alpha = 0.1$. Fig. 7b shows the same for $\alpha = 0.001$. The same scale is used for both figures. We see that the Mach number is mildly transonic in Fig. 7a while it is subsonic in Fig. 7b. Only the $\alpha = 0.1$ case has a transonic component in the poloidal directions, whereas the poloidal flows for $\alpha = 0.03$, $\alpha = 0.01$, $\alpha = 0.005$, and $\alpha = 0.001$ remain subsonic (see figs. 5a and 5b) (Fisker & Balsara 2005).

3.4. Hydrodynamic Instability in the Boundary Layer

The present simulations are based on an alpha-viscosity formulation, which implicitly assumes an underlying model for the sub-scale turbulence. However, the material that accretes on to a white dwarf has very low viscosity. Observations have not revealed the existence of magnetic fields at the WD surface. Besides, the radial gradient of the angular velocity has the wrong sign for the MRI to act. It is, therefore, interesting to explore the role of other hydrodynamical instabilities at the surface of the star. It is important to remember that the alpha-viscosity formulation does smear the velocity gradients. Yet, if these gradients are amenable to the development of a persistent hydrodynamical instability then the simulation should reveal its existence to us. It is in that spirit that we try to identify an instability that might give rise to a sub-scale hydrodynamical turbulence on an accreting white dwarf's surface.

There are several instabilities that can possibly lead to turbulence in boundary layers, such as the centrifugal instability (Rayleigh's criterion), the shearing Kelvin-Helmholtz instability, or even the Rayleigh-Taylor instability (buoyancy forces). Depending on the exact

Fig. 6.— Toroidal (ϕ) velocity in the disk's midplane shows the extent of the boundary layer as well as the sound speed after 3/4 of a Keplerian rotation period. Note that v_ϕ asymptotes to a higher value than $c_{s,\alpha}$.

angular velocity profile, pressure and density gradients each of the forces involved compete, some are stabilizing while other are destabilizing. The sufficient condition for linear stability of a rotating, radially stratified fluid under the influence of (a radial) gravity was given by Sung (1974)

$$\frac{1}{\rho} g_{eff} S_{\varpi} + \frac{k_z^2}{M} \Phi - \frac{1}{4} \frac{m^2}{M} \left(\frac{d\Omega}{d\varpi} \right)^2 \geq 0, \tag{8}$$

where, m and k_z are the angular and vertical mode numbers (in cylindrical coordinates (ϖ, ϕ, z)), M is defined as $M = k_z^2 + m^2/\varpi^2$, g_{eff} is the effective gravity defined as

$$g_{eff} = \frac{GM}{\varpi^2} - \varpi \Omega^2;$$

S_{ϖ} is the Schwarzschild discriminant (Schwarzschild 1906)

$$S_{\varpi} = \left(\frac{d\rho}{d\varpi} \right)_{ad} - \left(\frac{d\rho}{d\varpi} \right),$$

in which

$$\left(\frac{d\rho}{d\varpi} \right)_{ad} = \frac{\rho}{\Gamma_1 p} \frac{dp}{d\varpi}$$

is the adiabatic density gradient; and Φ is the Rayleigh discriminant (Rayleigh 1880, 1916)

$$\Phi = \frac{1}{\varpi^3} \frac{d}{d\varpi} \left(\varpi^2 \Omega \right)^2.$$

In the present case we do not consider vertical modes k_z and only consider the equatorial flow for which $r = \varpi$. There are two distinct cases as follows.

The axi-symmetric case (mode $m = 0$) gives the Solberg-Høiland criterion (Sung 1974, 1975)

$$\frac{1}{\rho} g_{eff} S_r + \Phi \geq 0.$$

The perturbations of an accretion disk to a convective instability has already been studied in this context (Livio & Shaviv 1977; Rüdiger et al. 2002; Johnson & Gammie 2006). In the limit of vanishing rotational velocity, the Solberg-Høiland criterion simply leads to the classical Schwarzschild condition $S_r > 0$ (Lebovitz 1965, 1966), which is also the condition in

Fig. 7.— (a) Left panel. This figure shows the poloidal Mach number with poloidal velocity vectors overlaid for model v1 after one Keplerian rotation. (b) Right panel. This figure shows the poloidal Mach number with poloidal velocity vectors overlaid for model v5 after one Keplerian rotation.

the vertical direction in the disk (Livio & Shaviv 1977). In the limit of a vanishing gradient of the density, the Solberg-Høiland criterion simplifies to Rayleigh's criterion for rotating fluids. The axi-symmetric instability in the boundary layer could possibly lead to a ring-like structure oscillating and in many ways similar to the "breathing" mode of an unstable star. This mode will not lead to turbulence, but could it explain the short period oscillations observed in CVs? The mode would depend on the density, temperature and rotation rate (Solberg-Høiland criterion), and its period and coherence would vary with these parameters. However, dwarf nova oscillations (DNOs) in CVs exhibit a 180deg phase jump at eclipse (Patterson 1979), and frequency doubling (presence of the first harmonic Patterson (1981), and therefore they cannot be explained by an $m = 0$ mode. On the other hand, Quasi-periodic oscillations (QPOs) in CVs do not all exhibit the same characteristics (some are believed to form at larger radii in the disk), and, therefore, we cannot completely rule out the $m = 0$ mode in the boundary layer as an additional mechanism to produce quasi-periodic oscillations (QPOs).

We now turn our attention to the non-axisymmetric case. In the case $m \neq 0$, a sufficient condition for stability that does not involve k_z is (Sung 1974)

$$\frac{1}{\rho} g_{eff} S_r - \frac{1}{4} r^2 \left(\frac{d\Omega}{dr} \right)^2 \geq 0. \tag{9}$$

This condition is usually written in the form of a modified Richardson number

$$R_i = g_{eff} \left(\frac{1}{\Gamma_1 p} \frac{dp}{dr} - \frac{1}{\rho} \frac{d\rho}{dr} \right) \left(r \frac{d\Omega}{dr} \right)^{-2} \geq \frac{1}{4}. \tag{10}$$

This is a generalization of the Miles-Howard theorem (Miles (1961); Howard (1961); see also Chimonas (1970)). The Miles-Howard theorem itself reduces to the original Richardson criterion (Richardson 1920) when compressibility is omitted and the Schwarzschild discriminant is replaced by the buoyancy term alone. The modified Richardson number was considered in a few analytical studies to analyze the stability of material accreting on the surface of a white dwarf (Durisen 1977; Kippenhahn & Thomas 1978; Livio & Truran 1987). Here, we have the opportunity to use results from numerical simulations to evaluate the modified Richardson number in the boundary layer. Using the definition of the Ledoux discriminant (Ledoux & Walraven 1958),

$$A = \frac{1}{\Gamma_1} \frac{d\ ln\ P}{dr} - \frac{d\ ln\ \rho}{dr},$$

the (modified) Richardson condition for stability is then written

$$R_i = N_{BV}^2 \left(r \frac{d\Omega}{dr} \right)^{-2} \geq \frac{1}{4}, \tag{11}$$

where A is related to the buoyancy (or Brunt-Väisälä) frequency N_{BV} (Pesnell 1986; Livio & Truran 1987, e.g.)

$$N_{BV}^2 = g_{eff} A.$$

The the flow is unstable for $R_i < 1/4$. In Fig.8 we show the Richardson number, R_i in the ϕ-direction (eqs. 10, 11), for run 91 and 95. The Richardson number is smaller than 1/4 in most of the domain and therefore the flow is unstable. It is important to remark that while the shear could stabilize the flow (Johnson & Gammie 2006), internal gravity waves can be reflected from a shear layer (Van Duin & Kalder 1982), and can be over-reflected from a rigid boundary (Shachdev & Satya Narayanan 1982). It has also been shown that modes can be unstable at the star-disk interface due to the propagation through the corotation (Tsang & Lai 2009). Unstable modes could be trapped and grow between (i) the surface of the WD and the strong shear region; and/or (ii) between the strong shear region and the corotation radius at larger radii in the inner disk, in a manner similar to the Papaloizou-Pringle instability (Papaloizou & Pringle 1984, 1985, 1987) observed in simulations of disks with a rigid inner boundary (Godon 1997a). The question of how the instability will develop cannot be addressed without full 3D simulations, which are beyond the scope of this work. However, a Richardson number $< 1/4$ in the boundary layer region and *at* the stellar surface raises the possibility of an instability. This instability could develop in the form of waves in the "spread layer" as studied by Piro & Bildsten (2004b) to explain DNOs in CVs, and raises the possibility of strong mixing between the hydrogen rich freshly accreted material and the WD material.

3.5. Formation of surface gravity waves

For the $\alpha = 0.1$ case, the outer edge of the boundary layer (where $d\Omega/dr \sim 0$) is located at $1.06r_*$. At $r = 1.03r_*$, v_ϕ is about 92% of v_K. This means that only 84% of the gravitational pull is supported by the centrifugal force while the rest is supported by pressure. The pressure for $\alpha = 0.1$ is illustrated in fig.4a and comes from the build up of density due to the high accretion rate facilitated by the high viscosity which drags down material from the disk and also keeps it from moving rapidly towards the poles once it makes contact with the WD surface. This results in a dense band at the foot point of the disk which causes a surface gravity wave of surface matter to spread towards the poles. Such surface

Fig. 8.— The toroidal Richardson Number R_ϕ as a function of the radius r in the equatorial plane ($\theta = 90°$), for run 91 and 95. The stellar radius is located at $r = 9 \times 10^8$cm. In most of the domain the Richardson number is smaller than 1/4.

gravity waves have been studied in the context of terrestrial physics by Miles (1957) and the role of turbulence in exciting these waves has also been studied Phillips (1957) and the simulations show a similar phenomenon on the surface of strongly accreting white dwarfs. The matter inflow is, however, sufficiently large to cause the disk material to overflow the gravity wave supersonically as described above and shown in fig.5a. Our present simulations do not show any evidence of wave breaking. However, should wave breaking reveal itself in simulations where the accretion is more vigorous, it would provide a further mechanism for directly mixing accreted material with the CNO-rich material that lies beneath the surface of the white dwarf.

The propensity for the creation of gravity waves and their magnitude decreases rapidly with lower values of α. Even for $\alpha = 0.03$, the effect is only marginal and for lower values it is no longer present. The effect is thus only present for large values of α, and possibly during dwarf novae in the outburst stage. Furthermore the gravity wave might be transient as the surface adjusts to a fluctuations in the accretion rate. For lower values of α, the matter accretes slowly inwards and spreads towards the poles in a uniformly thick layer.

3.6. Dissipative heating of the BL

The local rate of energy dissipation depends on the divergence of the angular velocity (Mihalas & Mihalas 1984), so fig.6 also indirectly shows where heat is released. Fig.9a shows that the supersonic impact of the accretion flow dissipates the most energy. However, energy is also dissipated at the interface between the BL and the surface. This is better seen in Fig.9b which shows that the toroidally rotating matter dissipates rotational kinetic energy along its entire interface with the surface as it slides against it.

In situations where the BL is optically thin, the radiation will be emitted from the very same regions where the heat is generated in fig. 6b. This may explain the optically thin BL and line emission seen in observations of U Gem during the quiescent phase (see also: Fisker & Balsara (2005)). Even in outburst, Fig. 3 shows that the optically thick boundary layer has an optical depth of 100. We therefore expect that the radiative diffusion of the heat in the radial direction will be faster than its advection in the poloidal direction. Consequently, our simulations provide a dynamically consistent reason for the formation of a warm belt of accreted matter, as was suggested in the observations of Sion et al. (2005) and the modeling of Godon & Sion (2005).

4. Summary and Conclusion

We have numerically simulated the structural dynamics of the BL for an accreting white dwarf surrounded by an α-disk for different values of α. The structure and dynamics of the BL is important, because it determines the specifics of the radiated spectrum that is emitted from this region. The energy radiated from the BL could account for up to half of the total energy released in the accretion process. For high values of α, the BL is optically thick and extends more than 30 degrees to either side of the disk plane after 3/4 of a Keplerian rotation period (t_K=19s).

The simulations also show that high values of α result in a spreading BL which sets off gravity waves in the surface matter. The accretion rate can be high enough in the high α cases to cause a depression to form on the surface of the star. The accretion flow moves supersonically over the depression that is formed, making it susceptible to the rapid development of gravity wave and/or Kelvin-Helmholtz instabilities. The low viscosity cases also show a spreading BL, but here the accretion flow does not set off gravity waves and it is optically thin.

We argued in the paper by Sion et al. (2005) that an accretion belt might be sustained after a long period of perhaps thousands of dwarf nova events such that an equilibrium or steady state is established between the Richardson number and the average rate of accretion. Our 2D simulations in this paper has not been followed long enough for any steady state behavior to be observed. Therefore, it may be premature for us on the basis of the limited extent of these first simulations to argue in favor or against the formation of an accretion belt.

If the boundary layer remains optically thick following an episode of high accretion, this could explain the "second components" of FUV flux seen in several dwarf novae during quiescence. It should also be pointed out that a hot equatorial accretion region could persist even after the material has reached co-rotation with the white dwarf. For example, a hot (50,000K) region of low rotation is seen in successive HUT spectra of U Gem taken early after an outburst and very late after the same outburst.

The susceptibility of the flow in the boundary layer to undergo a purely hydrodynamic

Fig. 9.— (a) Left panel. A logarithmic color plot of the dissipation rate for the $\alpha = 0.1$ case after 3/4 of a Keplerian rotation period. (b) Right panel. A logarithmic color plot of the dissipation rate for the $\alpha = 0.001$ case after 3/4 of a Keplerian rotation period. Notice that the color scale is different for fig. 8a.

instability (modified Richardson number $< 1/4$) was found assuming an *a priori* alpha viscosity parametrization consistent with that of the disk. The unstable flow would be very effective in mixing of the accreted material with the outer layer (few scale heights) of the WD envelope. However, it has been shown (Papaloizou & Szuszkiewicz 1994; Narayan et al. 1994; Kato & Inagaki 1994; Godon 1995) that the turbulent viscosity law for a non-Keplerian disk cannot be represented by the standard alpha viscosity prescription (α =constant), as alpha is proportional to the shear (Godon 1995; Abramowicz et al. 1996)

$$\alpha \propto \partial\Omega/\partial r.$$

Even more so, in the boundary layer, the turbulent viscosity is proportional to the square of the turbulent Mach number $\mathcal{M}_t^2$ (Shakura & Sunyaev 1988; Godon 1995), which decreases quickly for for subsonic turbulence (supersonic turbulence quickly dissipated due to shocks)

$$\nu_{BL} = \alpha_{BL} c_s H, \qquad \alpha_{BL} = \alpha \mathcal{M}_t^2 \frac{\delta_{BL}}{H} \frac{c_s}{v_K - v_*}.$$

Supersonic radial infall in the boundary layer also leads to a smaller turbulent viscosity as shown by (Papaloizou & Szuszkiewicz 1994; Narayan et al. 1994; Kato & Inagaki 1994; Godon 1995), and the formulation of such a viscosity can also be obtained considering causality in one-dimensional steady-state models of accretion disk boundary layers (Popham & Narayan 1992), namely the radial infall viscosity cannot be larger than the maximum speed of the turbulence. In that case one has (Godon 1995)

$$\nu_{BL} = \alpha_{BL} c_s H, \qquad \alpha_{BL} = \alpha \frac{\delta_{BL}}{H} \frac{1}{\mathcal{M}_r^3},$$

where $\mathcal{M}_r > 1$ is the radial infall Mach number, and it is smaller than the turbulent Mach number $\mathcal{M}_t$ (see also Popham & Narayan (1992)).

In these regions close to the stellar surface (and even more so away from the equatorial region), one can use a viscosity of the form

$$\nu \propto (v - v_*) z, \tag{12}$$

where v_* is the stellar rotational velocity, v is the velocity of the flow, and z is the distance from the surface of the WD. It is clear that such a viscosity would decrease rapidly as $z \to 0$, and would agree with the fact that the size of the turbulent Eddies be limited by the presence of the stellar surface and their velocity proportional to the change of v over a distance z (see also Landau & Lifshitz (1987)).

Piro and Bildsten have shown that the properties of the boundary ("spread") layer vary depending on the value of the viscosity, however, like us, they assume an alpha viscosity in

which alpha is not a function of the coordinates, the radial infall velocity or or the shear. It is our aim, in future simulations, to carry out simulation of the boundary layer, by assuming a viscosity law that is greatly reduced in the boundary layer. For this purpose, one could use a combination of viscosity prescriptions suggested in the above mentioned works. Since the results presented here as well as Piro & Bildsten's results depend strongly on the value of α (which was assumed to be constant), it is clear that a modified alpha viscosity prescription can lead to some new and unexpected results.

The evolutionary simulations presented here, while followed for only a brief interval of time, represent the first successful, fully hydrodynamic treatment of the the flow of accreted matter *into* the white dwarf surface layers. All previous attempts to follow accretion hydrodynamically from the boundary layer into the white dwarf surface layers were either not computationally viable or the underlying white dwarf was treated as a solid boundary.

The successful convergence of our dynamical model simulations opens the door to going well beyond this first stage and ultimately follow the dynamical evolution over much longer time intervals for both the high viscosity and low viscosity cases with the inclusion of radiative processes.

PG wishes to thank Steve Lubow for a discussion on the importance of the adiabatic term in the modified Richardson number, and Mario Livio for his kind hospitality at the Space Telescope Science Institute. This work is supported by NASA ATFP grant NNX08AG69G to Villanova University and the University of Notre Dame. Participation by EMS and PG was also supported in part by NSF grant AST08-07892 and NASA ADP grant NNX04GE78G to villanova University.

A. Numerical model

The source of the angular momentum transport in the BL is a combination of magnetic fields and turbulence. However, an a priori prescription, in particular in the BL, is a source of disagreement (see Popham & Narayan (1995) and references therein). Instead the efficiency of the angular momentum transport can be parametrized with a coefficient, α (Shakura & Sunyaev 1973). Describing the angular momentum transport with a simple shear coefficient means that the dynamics follows the Navier-Stokes equations. Here the Navier-Stokes equations are solved in spherical coordinates $i = (r, \theta, \phi)$ as given by Mihalas & Mihalas (1984). The accelerations are defined by the time-derivative of the ve-

locities which are given in spherical coordinates.

$$\begin{aligned}
\rho a_r &= -\frac{GM\rho}{r} - \frac{\partial p}{\partial r} + \frac{\partial}{\partial r}\left[2\mu\frac{\partial v_r}{\partial r} + \left(\zeta - \frac{2}{3}\mu\right)(\nabla\cdot v)\right] + \frac{1}{r}\frac{\partial}{\partial\theta}\left\{\mu\left[r\frac{\partial}{\partial r}\left(\frac{v_\theta}{r}\right) + \frac{1}{r}\frac{\partial v_r}{\partial\theta}\right]\right\} \\
&+ \frac{1}{r\sin\theta}\frac{\partial}{\partial\phi}\left\{\mu\left[\frac{1}{r\sin\theta}\frac{\partial v_r}{\partial\phi} + r\frac{\partial}{\partial r}\left(\frac{v}{v_\phi}\right)\right]\right\} \\
&+ \frac{\mu}{r}\left[4r\frac{\partial}{\partial r}\left(\frac{v_r}{r}\right) - \frac{2}{r\sin\theta}\frac{\partial}{\partial\theta}(v_\theta\sin\theta)\frac{2}{r\sin\theta}\frac{\partial v_\phi}{\partial\phi} + r\cot\theta\frac{\partial}{\partial r}\left(\frac{v_\theta}{r}\right) + \frac{\cot\theta}{r}\frac{\partial v_r}{\partial\theta}\right] \qquad \text{(A1)}
\end{aligned}$$

$$\begin{aligned}
\rho a_\theta &= -\frac{1}{r}\frac{\partial p}{\partial\theta} + \frac{\partial}{\partial r}\left\{\mu\left[r\frac{\partial}{\partial r}\left(\frac{v_\theta}{r}\right) + \frac{1}{r}\frac{\partial v_r}{\partial\theta}\right]\right\} + \frac{1}{r}\frac{\partial}{\partial\theta}\left[\frac{2\mu}{r}\left(\frac{\partial v_\theta}{\partial\theta} + v_r\right) + \left(\zeta - \frac{2}{3}\mu\right)(\nabla\cdot v)\right] \\
&+ \frac{1}{r\sin\theta}\frac{\partial}{\partial\phi}\left\{\mu\left[\frac{\sin\theta}{r}\frac{\partial}{\partial\theta}\left(\frac{v_\theta}{\sin\theta}\right) + \frac{1}{r\sin\theta}\frac{\partial v_\phi}{\partial\phi}\right]\right\} + \frac{\mu}{r}\left\{\frac{2\cot\theta}{r}\left[\sin\theta\frac{\partial}{\partial\theta}\left(\frac{v_\theta}{\sin\theta}\right) - \frac{1}{\sin\theta}\frac{\partial v_\phi}{\partial\phi}\right]\right. \\
&+ \left. 3r\frac{\partial}{\partial r}\left(\frac{v_\theta}{r}\right) + \frac{3}{r}\frac{\partial v_r}{\partial\theta}\right\} \qquad \text{(A2)}
\end{aligned}$$

$$\begin{aligned}
\rho a_\phi &= -\frac{1}{r\sin\theta}\frac{\partial p}{\partial\phi} + \frac{\partial}{\partial r}\left\{\mu\left[\frac{1}{r\sin\theta}\frac{\partial v_r}{\partial\phi} + r\frac{\partial}{\partial r}\left(\frac{v_\phi}{r}\right)\right]\right\} + \frac{1}{r}\frac{\partial}{\partial\theta}\left\{\mu\left[\frac{\sin\theta}{r}\frac{\partial}{\partial\theta}\left(\frac{v_\phi}{\sin\theta}\right) + \frac{1}{r\sin\theta}\frac{\partial v_\theta}{\partial\phi}\right]\right\} \\
&+ \frac{1}{r\sin\theta}\frac{\partial}{\partial\phi}\left[\frac{2\mu}{r}\left(\frac{1}{\sin\theta}\frac{\partial v_\phi}{\partial\phi} + v_R + V_\theta\cot\theta\right) + \left(\zeta - \frac{2}{3}\mu\right)(\nabla\cdot v)\right] \\
&+ \frac{\mu}{r}\left\{\frac{3}{r\sin\theta}\frac{\partial v_r}{\partial\phi} + 3r\frac{\partial}{\partial r}\left(\frac{v_\phi}{r}\right) + 2\cot\theta\left[\frac{\sin\theta}{r}\frac{\partial}{\partial\theta}\left(\frac{v_\theta}{\sin\theta}\right) + \frac{1}{r\sin\theta}\frac{\partial v_\theta}{\partial\phi}\right]\right\} \qquad \text{(A3)}
\end{aligned}$$

Here a_i are the accelations, p is the pressure, and ζ is the coefficient of bulk viscosity, which we set to zero to treat the fluid as a Maxwellian fluid. The kinematic viscosity $\nu = \mu/\rho$ is set by the alpha-disk prescription of Shakura & Sunyaev (1973), so $\nu = \alpha c_s H$, where H is the disk scale height which should properly correspond to the turbulent turnover scale with convective bubbles moving at sound speed c_s.

The viscous dissipation function is given by

$$\begin{aligned}
\Phi &= 2\mu\left\{\left(\frac{\partial v_r}{\partial r}\right)^2 + \left(\frac{1}{r}\frac{\partial v_\theta}{\partial\theta} + \frac{v_r}{r}\right)^2 + \left(\frac{1}{r\sin\theta}\frac{\partial v_\phi}{\partial\phi} + \frac{v_r}{r} + \frac{v_\theta\cot\theta}{r}\right)^2\right. \\
&+ \frac{1}{2}\left[r\frac{\partial}{\partial r}\left(\frac{v_\theta}{r}\right) + \frac{1}{r}\frac{\partial v_r}{\partial\theta}\right]^2 + \frac{1}{2}\left[r\frac{\partial}{\partial\phi}\left(\frac{v_\phi}{r}\right) + \frac{1}{r\sin\theta}\frac{\partial v_r}{\partial\phi}\right]^2 + \left.\frac{1}{2}\left[\frac{\sin\theta}{r}\frac{\partial}{\partial\theta}\left(\frac{v_\phi}{\sin\theta}\right) + \frac{1}{r\sin\theta}\frac{\partial v_\theta}{\partial\phi}\right]^2\right\} \\
&+ \left(\zeta - \frac{2}{3}\mu\right)\left[\frac{1}{r^2}\frac{\partial}{\partial r}(r^2 v_r) + \frac{1}{r\sin\theta}\frac{\partial}{\partial\theta}(v_\theta\sin\theta) + \frac{1}{r\sin\theta}\frac{\partial v_\phi}{\partial\phi}\right]^2 . \qquad \text{(A4)}
\end{aligned}$$

The dissipation function enters the heat equation as

$$\rho\left[c_v\frac{dT}{dt} + p\frac{d}{dt}\left(\frac{1}{\rho}\right) - \frac{GM}{r}\right] = \Phi - \nabla\cdot\vec{q} \qquad \text{(A5)}$$

where T is the temperature, $c_v = R/(\gamma - 1)$ is the specific heat capacity. As mentioned in section 2, the heat equations does not contain transport terms, so $\vec{q} \equiv 0$. This means that dissipated heat can only be lost be pressure work. Conversely, if the dissipation term is neglected as is the case in the optically thin limit, the only way to change the temperature at any given point is through pressure work.

B. Computational domain setup

We set up an accretion disk around the WD. This setup comprises three parts: the disk, the stellar atmosphere and the halo. This improves on the previous simulations of Kley & Hensler (1987) which did not include a stellar atmosphere. For stability reasons it is important that the pressure of the three components match at their respective interfaces. This is to prevent shocks from dominating the solution. We have therefore carefully designed the domain to ensure the partial pressures are identical at the common interface.

The radius of the star is $r = 9000$km. We assume that the disk is symmetric in the plane and that is it axisymmetric. We use the model of Balsara (2004). In their notation, we have $a = 1/2$ and $\gamma = 5/3$, so their model effectively reduces to a constant density in the disk plane for our case. We assume the the initial halo, atmosphere and disk are isothermal and obey the polytropic equation of state

$$P = K\rho^{\gamma} \tag{B1}$$

We set $\rho_0 = 1.2 \times 10^{-5}\mathrm{gcm}^{-3}$. Setting a temperature for the disk then fully determines K. Above the disk plane the partial pressure of the disk matter follows the prescription of a plane parallel atmosphere where the pressure falls off with the e-folding distance given by the scale height. The density is calculated according to eq. [B1] (see Landau & Lifshitz (1987).

The temperature of the WD is set to $T_* = 300000$K. The atmospheric scale height is given by $H = RT_*/g\mu$, where $g = GM/r^2$, R is the gas constant and μ is the mean molecular weight. The inner boundary of the computational domain is set to $r_* - 5H_*$. The disk scale height is given by $H_d = c_s\sqrt{r/g}$, where $c_s = \sqrt{\gamma P/\rho}$ is the local sound speed. The outer boundary of the computational domain is set to $r_* + 3H_d$. The disk is set up with a Keplerian velocity profile. The disk temperature is set to $T_d = 1000000$K. Pressure matching between the disk and the stellar atmosphere is achieved by selecting ρ_* so that $P_* \equiv P_d$ at the base of the disk at $r = r_*$. The pressure profile of the WD atmosphere follows the standard solution of a plane parallel atmosphere (see Landau & Lifshitz (1987))

In these models we do not have a self-consistent disk corona, which would provide pressure balance at the upper boundary of the accretion disk. For that reason, we use a

very hot, initially static halo that provides pressure balance both to the upper boundary of the disk as well as to the WD's atmosphere. The halo's temperature is chosen to be high enough that the mass in the halo is less than the mass in the disk or the WD atmosphere by a factor of 35, making it dynamically unimportant. The temperature of the halo is set so $T_h = 50T_d$. The scale height of the halo is determined by the gravitational component in the z-direction. The density of the halo is set to match the pressure of the disk one disk scale height above the disk base at r_*.

The careful pressure matching described above ensures that the dynamical instabilities at $t = 0$ are negligible. Therefore, the computational model will quickly stabilize to a dynamical equilibrium.

REFERENCES

Abramowicz, M., Brandenburg, A., & Lasota, J.-P. 1996, MNRAS, 281, L21

Alexakis, A., et al. 2004, ApJ, 602, 931

Balbus, S. A., Gammie, C. F., & Hawley, J. F. 1994, MNRAS, 271, 197

Balsara, D. S. 1998a, ApJS, 116, 119

—. 1998b, ApJS, 116, 133

—. 2004, ApJS, 151, 149

Balsara, D.S., & Fisker, J.L., 2005, in Protostars and Planets V, p. 8631

Balsara, D. S., & Shu, C.-W. 2000, J. Comput. Phys., 160, 405

Balsara, D. S., & Spicer, D. S. 1999a, J. Comput. Phys., 148, 133

—. 1999b, J. Comput. Phys., 148, 133

Bath, G.T. 1972, ApJ, 173, 121

Becker, R.H., & Marshal, F.E. 1981, ApJ, 244, L93

Belloni, T. et al. 1991, A&A, 246, L44

Beuermann, K., & Thomas, H.-C. 1993, Adv.Space Res., 13, 115

Bhatia, P.K. 1974, Ap&SS, 26, 319

Brandenburg, A., Lasota, J.-P., & Abramowicz, M. 1996, MNRAS, 281, L21

Cannizzo, J. K., Shafter, A.W., & Wheeler, J.C. 1988, ApJ, 333, 227

—. 1998, ApJ, 493, 426

Chandrasekhar, S. 1961, Hydrodynamic and Hydromagnetic Stability, Oxford, Clarendon Press

Cheng, F.H., Sion, E.M., Szkody, P., Huang, M. 1997, ApJ, 484, L149

Chimonas, G. 1970, J.Fluid Mech., 43, 833

Collins, T. J. B., Helfer, H. L., & Horn, H. M. V. 1998, ApJ, 508, L159

Córdova, F.A., Chester, T.J., Tuohy, I.R., & Garmire, G.P. 1980, ApJ, 235, 163

Córdova, F.A., Mason, K.O., & Nelson, J.E. 1981, ApJ, 245, 609

Córdova, F.A., & Mason, K.O. 1983, in: Accretion-Driven Stellar X-ray sources, eds. W.Lewin, E.van den Heuvel, CUP 1983, p.147

Crawford, J.A., & Kraft, R.P. 1956, ApJ, 123, 44

Drazin, P.G., & Reid, W.H., 1981, *Hydrodynamic Stability*, Cambridge University Press, Cambridge

Dubrulle, B. 1993, Icarus, 106, 59

Durisen, R. H. 1973, ApJ, 183, 205

—. 1977, ApJ, 213, 145

Ferland, G. J., Langer, S. H., MacDonald, J., Pepper, G. H., Shaviv, G., & Truran, J. 1982, ApJ, 262, L53

Fisker, J. L., & Balsara, D. S. 2005, ApJ, 635, L69

Flannery, B.P. 1974, MNRAS, 170, 325

Frank, J., King, A., & Raine, D. 2002, Accretion Power in Astrophysics, 3rd edn. (Cambridge: Cambridge University Press)

Froning, C. S., Long, K. S., Drew, J. E., Knigge, C., & Proga, D. 2001, ApJ, 562, 963

Glasner, S. A., Livne, E., & Truran, J. W. 1997, ApJ, 475, 754

Godon, P. 1995, MNRAS, 277, 157

—. 1996a, ApJ, 462, 456

—. 1996b, MNRAS, 282, 1107

—. 1997a, ApJ, 480, 329

—. 1997b, ApJ, 483, 882

Godon, P., Regev, O., and Shaviv, G. 1995, MNRAS, 275, 1093

Godon, P., & Sion, E. M. 2002, ApJ, 566, 1084

—. 2003, ApJ, 586, 427

—. 2005, MNRAS, 361, 809

Godon, P., Sion, E. M., Cheng, F., Gänsicke, B. T., Howell, S., Knigge, C., Sparks, W. M., & Starrfield, S. 2004a, ApJ, 602, 336

Godon, P., Sion, E.M., Cheng, F.H., Szkody, P., Long, K.S., Froning, C.S. 2004b, ApJ, 612, 429

Hack, M., & la Dous, C. 1993, Cataclysmic Variables and Related Objects, Monograph series on nonthermal phenomenon in stellar atmospheres, NASA SP-507, Washington

Hamilton, J.M., & Habernathy, F.H. 1994, J.Fluid Mech., 264, 185

Hoare, M.G., & Drew, J.E. 1991, MNRAS, 249, 452

Howard, L.N. 1961, J.Fluid Mech., 10, 509

Inogamov, N. A., & Sunyeav, R. 1999, Astron. Lett., 25, 269

Jiang, G.-S., & Shu, C.-W. 1996, J. Comput. Phys., 126, 202

Johnson, B.M., & Gammie, C.F. 2006, ApJ, 636, 63

José, J. 2005, Nucl. Phys., A758, 713

Kato, S., & Inagaki, S. 1994, PASJ, 46, 289

King, A. 1997, MNRAS, 288, 16

King, A.R., & Shaviv, G. 1984, Nature, 308, 519

Kippenhahn, R., & Thomas, H.-C. 1978, A&A, 63, 265

Kley, W. 1989, A&A, 208, 98

—. 1991, A&A, 247, 95

Kley, W., & Hensler, G. 1987, A&A, 172, 124

Kley, W., & Lin, D.N.C. 1996, ApJ, 461, 933

—. 1999, ApJ, 518, 833

Kluźniak, W. 1987, Ph.D. Thesis, Stanford University

Kraft, R.P. 1962, ApJ, 135, 408

Landau, L. D., & Lifshitz, E. M. 1987, Fluid mechanics (New York: Pergamon Press)

Lebovitz, N.R. 1965, ApJ, 142, 229

—. 1966, ApJ, 146, Notes 946

Ledoux, P., & Walraven, Th. 1958, *Handbuch der Physik*, 41, ed. S. Flügge (Berlin: Springer-Verlag), 353

Livio, M., & Pringle, J.E. 1992, MNRAS, 259, P23

—. 1998, ApJ, 505, 339

Livio, M., & Shaviv, G. 1977, A&A, 55, 95

Livio, M., & Truran, J.W. 1987, ApJ, 318, 316

Long, K. S., Blaier, W. P., Bowyers, C. W., Sion, E. M., & Hubeny, I. 1993, ApJ, 405, 327

Lubow, S.H., & Shu, F.H. 1975, ApJ, 198, 383

Lynden-Bell, D., & Pringle, J. E. 1974, MNRAS, 168, 303

MacDonald, J. 1983, ApJ, 273, 289

Mauche, C.W. 1996, in: Proceedings of X-Ray Imaging and Spectroscopy of Comic Hot Plasmas, Ed.F.Makino

—. 2004, ApJ, 610, 422

Mauche, C.W., Raymond, J.C., & Mattei, J.A. 1995, ApJ, 446, 842

Mauche, C.,W., Wade, R.A., Polidan, R.S., van der Woerd, H., & Paerels, F.B.S. 1991, ApJ, 372, 659

Meyer, F., & Meyer-Hofmeister, E. 1982, A&A, 106, 34

—. 1994, A&A, 288, 175

Mihalas, D., & Mihalas, B. W. 1984, Foundations of radiation hydrodynamics (Cambridge: Cambridge Univ. Press)

Miles, J.W. 1957, J. Fluid Mech., 3, 185

—. 1961, J. Fluid Mech., 10, 496

Mukai, K., & Patterson, J. 2004, RM AC 20, 244

Mukai, K., Wood, J.H., Naylor, T., Schlegel, E.M., & Swank, J.H. 1997, ApJ, 475, 812

Narayan, R., Loeb, A., & Kumar, P. 1994, ApJ, 431, 359

Narayan, R. & Popham, R. 1993, Nature, 362, 820

Obach, C. & Glatzel, W. 1999, MNRAS, 303, 603

Orszag, S.A., & Kell, L.C. 1980, J.Fluid Mech., 96, 159

Pandel, D., Córdova, F.A., & Howell, S.B. 2003, MNRAS, 346, 1231

Pandel, D., Córdova, F.A., Mason, K.O., & Priedhorsky, W.C. 2005, ApJ, 626, 396

Papaloizou, J.C.B., & Pringle, J.E. 1984, MNRAS, 208, 721

—. 1985, MNRAS, 213, 799

—. 1987, MNRAS, 225, 267

Papaloizou, J.C.B., & Stanley, G.Q.G. 1986, MNRAS, 220, 593

Papaloizou, J.C.B., & Szuszkiewicz, E. 1994, MNRAS, 268, 29

Patterson, J. 1979, ApJ, 234, 978

Patterson, J. 1981, ApJS, 45, 517

Patterson, J., & Raymond, J.C. 1985, ApJ, 295, 550

Phillips, O.M. 1957, J. Fluid Mech., 2, 417

Pesnell, W.D. 1986, ApJ, 301, 204

Piro, A. L., & Bildsten, L. 2004a, ApJ, 610, 977

Piro, A. L., & Bildsten, L. 2004a, ApJ, 616, L155

Piro, A.L., Arras, P., & Bildsten, L. 2005, ApJ, 628, 401

Polidan, R.S., Mauche, C.S., & Wade, R.A. 1990, ApJ, 356, 211

Ponman, T.J., Belloni, T., Duck, S.R., Verbunt, F., Watson, M.G., Wheatley, P.J., & Pfeffermann, E. 1995, MNRAS, 276, 495

Popham, R. 1997, ApJ, 478, 734

—. 1999, MNRAS, 308, 979

Popham, R., & Narayan, R. 1991, ApJ, 370, 614

—. 1992, ApJ, 394, 255

—. 1995, ApJ, 442, 337

Prendergast, K. H., & Burbidge, G. R. 1968, ApJ, 151, L83

Pringle, J. E. 1981, ARA&A, 19, 137

Pringle, J.E., & Savonije, G.J. 1979, MNRAS, 187, 777

Rayleigh, Lord, 1880, Proc.London Math.Soc., 11, 57

—. 1916, Proc.R.Soc.London, A., 93, 148

Regev, O. 1983, A&A, 126, 146

Regev, O., & Shara, M.M. 1989, ApJ, 340, 1006

Richardson, L.F. 1920, Proc.Roy.Soc.London A, 9F, 354

Ritter, H., & Kolb, U. 1998, A&AS, 129, 83

Robertson, J. A., & Frank, J. 1986, MNRAS, 221, 279

Roe, P. L., & Balsara, D. S. 1996, SIAM J. Appl. Math., 56, 57

Rose, W.K. 1968, ApJ, 152, 245

Rosner, R., Alexakis, A., Young, Y.-N., Truran, J. W., & Hillebrandt, W. 2001, ApJ, 562, L177

Rüdiger, G., Arlt, R., Shalybkov, D. 2002, A&A, 391, 781

Saric, W.S. 1994, Annu.Rev.Fluid Mech., 26, 379

Schwarzschild, K. 1906, Göttingen Nachr., 41

Shachdev, P.L., & Satya Narayanan, A. 1982, Indian J. Pure Appl.Math., 13, 989

Shakura, N. I., & Sunyaev, R. A. 1973, A&A, 24, 337

Shakura, N. I., & Sunyaev, R. A. 1988, Adv.Space Res., 8, 135

Shaviv, G. 1987, ApSS, 130, 303

Shaviv, G., & Starrfield, S. 1987, ApJ, 321, L51

Sion, E.M. 1995, ApJ, 438, 876

Sion, E. M., Cheng, F., Gänsicke, B., & Szkody, P. 2005, ApJ, 614, L61

Starrfield, S. 1971a, MNRAS, 152, 307

Starrfield, S. 1971b, MNRAS, 155, 129

Starrfield, S., Truran, J. W., Sparks, W. M., & Kutter, G. S. 1972, ApJ, 176, 169

Sung, C.H. 1974, A&A, 33, 99

—. 1975, Ap&SS, 26, 305

Szkody, P., Nishikida, K., Raymond, J. C., Seth, A., Hoard, D. W., Long, K. S., & Sion, E. M. 2002, ApJ, 574, 942

Tsang, D., & Lai, D. 2009, MNRAS, 396, 589

Tylenda, R. 1981, Acta Astronomica, 31, 267

Van Duin, C.A., & Kalder, H. 1982, J. Fluid Mech., 120, 505

van Teeseling, A. & Verbunt, F. 1994, A&A, 292, 519

van Teeseling, A. Beuermann, K., & Verbunt, F. 1996, A&A, 315, 467

Warner, B. 1987, MNRAS, 227, 23

—. 1995, Cataclysmic Variable Stars (Cambridge: Cambridge University Press)

Welsh, W. F., Sion, E. M., Godon, P., Gänsicke, B. T., Knigge, C., Long, K. S., & Szkody, P. 2003, ApJ, 599, 509

Zahn, J.-P. 1990, in Structure and Emission Properties of Accretion Disks, ed.C.Bertout, S.Collin-Souffrin, J.-P.Lasota, & V.J.Tran Than (Paris: Editions Frontières), 87

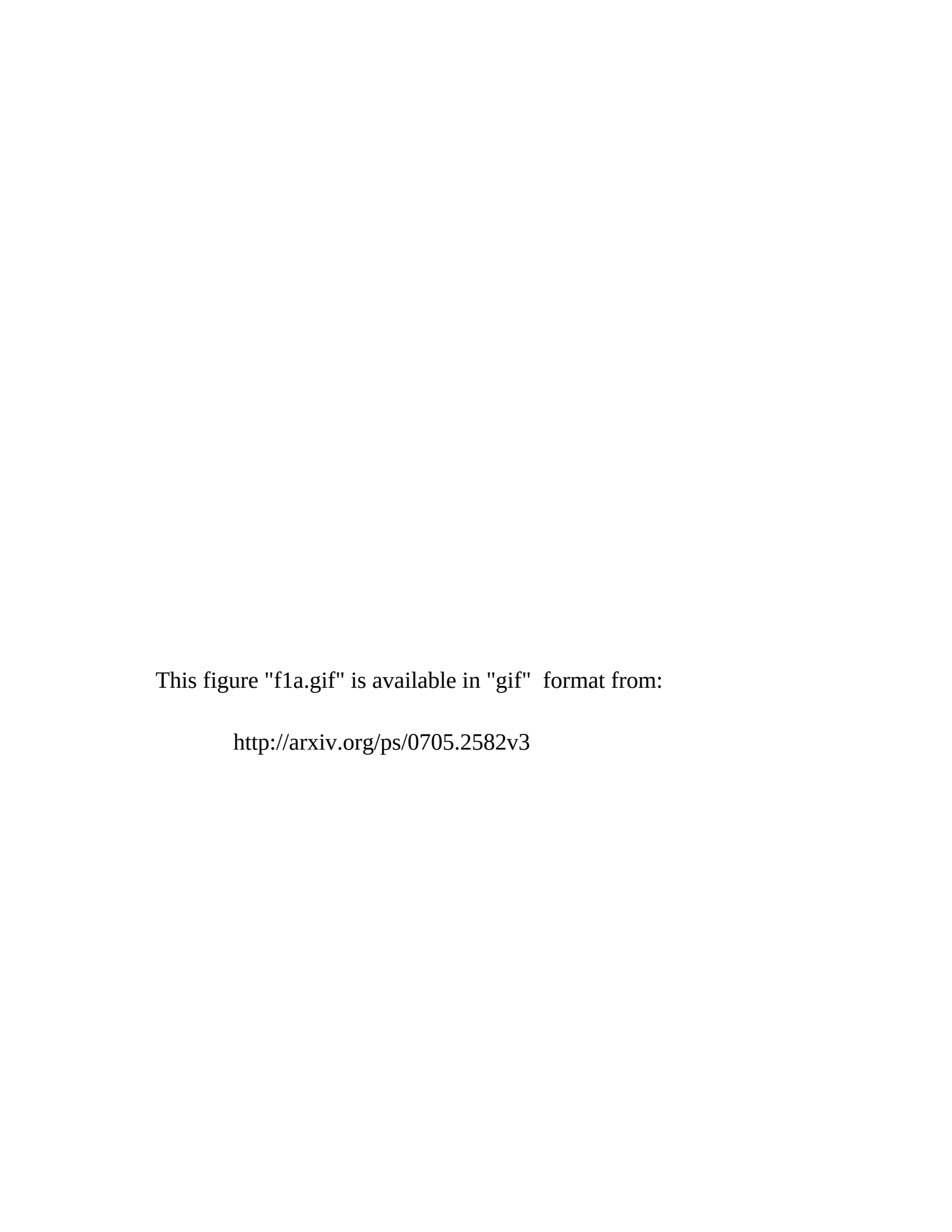
This figure "f1a.gif" is available in "gif" format from:
http://arxiv.org/ps/0705.2582v3

This figure "f1b.gif" is available in "gif" format from:

http://arxiv.org/ps/0705.2582v3

This figure "f1c.gif" is available in "gif" format from:

http://arxiv.org/ps/0705.2582v3

This figure "f1d.gif" is available in "gif" format from:

http://arxiv.org/ps/0705.2582v3

This figure "f2.gif" is available in "gif" format from:

http://arxiv.org/ps/0705.2582v3

This figure "f3.gif" is available in "gif" format from:

http://arxiv.org/ps/0705.2582v3

This figure "f4a.gif" is available in "gif" format from:

http://arxiv.org/ps/0705.2582v3

This figure "f4b.gif" is available in "gif" format from:

http://arxiv.org/ps/0705.2582v3

This figure "f4c.gif" is available in "gif" format from:

http://arxiv.org/ps/0705.2582v3

This figure "f4d.gif" is available in "gif" format from:

http://arxiv.org/ps/0705.2582v3

This figure "f5a.gif" is available in "gif" format from:

http://arxiv.org/ps/0705.2582v3

This figure "f5b.gif" is available in "gif" format from:

http://arxiv.org/ps/0705.2582v3

This figure "f6.gif" is available in "gif" format from:

http://arxiv.org/ps/0705.2582v3

This figure "f7a.gif" is available in "gif" format from:

http://arxiv.org/ps/0705.2582v3

This figure "f7b.gif" is available in "gif" format from:

http://arxiv.org/ps/0705.2582v3

This figure "f8.gif" is available in "gif" format from:

http://arxiv.org/ps/0705.2582v3

This figure "f9a.gif" is available in "gif" format from:

http://arxiv.org/ps/0705.2582v3

This figure "f9b.gif" is available in "gif" format from:

http://arxiv.org/ps/0705.2582v3